The Photophobic Receptor from *Natronobacterium pharaonis*: Temperature and pH Dependencies of the Photocycle of Sensory Rhodopsin II

Igor Chizhov, Georg Schmies, Ralf Seidel, Jens R. Sydor, Beate Lüttenberg, and Martin Engelhard

Max-Planck-Institut für Molekulare Physiologie, 44139 Dortmund, Germany

ABSTRACT   The photocycle of the photophobic receptor sensory rhodopsin II from *N. pharaonis* was analyzed by varying measuring wavelengths, temperature, and pH, and by exchanging H_2O with D_2O. The data can be satisfactorily modeled by eight exponents over the whole range of modified parameters. The kinetic data support a model similar to that of bacteriorhodopsin (BR) if a scheme of irreversible first-order reactions is assumed. Eight kinetically distinct protein states can then be identified. These states are formed from five spectrally distinct species. The chromophore states S_i correspond in their spectral properties to those of the BR photocycle, namely $pSRII_{510}$ (K), $pSRII_{495}$ (L), $pSRII_{400}$ (M), $pSRII_{485}$ (N), and $pSRII_{535}$ (O). In comparison to BR, $pSRII_{400}$ is formed ~10 times faster than the M state; however, the back-reaction is almost 100 times slower. Comparison of the temperature dependence of the rate constants with those from the BR photocycle suggests that the differences are caused by changes of ΔS. The rate constants of the pSRII photocycle are almost insensitive to the pH variation from 9.0 to 5.5, and show only a small H_2O/D_2O effect. This analysis supports the idea that the conformational dynamics of pSRII controls the kinetics of the photocycle of pSRII.

INTRODUCTION

Bacteria have evolved intricate signaling systems that enable them to respond adequately and efficiently to environmental challenges. An increasingly detailed picture of the underlying mechanisms has been obtained from the elucidation of the chemotactic behavior of Eubacteria such as *Escherichia coli* (reviewed in, e.g., Eisenbach, 1996). Similar signal transduction networks have also recently been identified in the archaeal species *Halobacterium salinarum* (reviewed in, e.g., Hoff et al., 1997). The machinery behind these signal transduction chains in both Eubacteria and Archaea is started by the binding of substrates to their specific membrane-bound receptors. The information is transferred across the plasma membrane to the cytoplasmic signaling domain, the activation of which triggers the subsequent signal processing. It includes amplification and integration of sensory inputs, as well as adaptation to a constant flux of stimuli.

The archaeal species *H. salinarum* has developed not only chemotactic but also phototactic signal transduction chains. The phototactic receptors sensory rhodopsin I (SRI) and sensory rhodopsin II (SRII) are closely related structurally, to each other and to the two other bacterial rhodopsins, the ion pumps bacteriorhodopsin (BR) and halorhodopsin (HR). All four bacterial pigments contain an all-*trans* retinal that is bound to the seven helical membrane protein via a protonated Schiff base. On light excitation of the retinyli-

dene chromophore, characteristic photoreaction cycles of the four pigments are observed, which are coupled to the physiological response, i.e., signal transduction or ion pumping. In the case of the sensory rhodopsins, the information "light" is specifically transferred to their corresponding halobacterial transducers of sensory rhodopsin (Htr), which possess a signal domain with considerable sequence similarities to the chemotactic methyl accepting proteins (MCPs) (Zhang et al., 1996; Seidel et al., 1995; Yao and Spudich, 1992).

Whereas the photocycles of bacteriorhodopsin and halorhodopsin have been the subject of numerous publications (reviewed in Lanyi and Váró, 1995, and Oesterhelt, 1995, respectively), much less is known about the sensory rhodopsins. This lack of data is especially true for the photophobic receptor SRII. The data available from low-temperature experiments and time-resolved absorption spectroscopy revealed a scheme which resembles that of the BR photocycle (Scharf et al., 1992b; Miyazaki et al., 1992; Imamoto et al., 1991, 1992b; Hirayama et al., 1992; Shichida et al., 1988). K-, L-, M-, and O-like species have been identified after photoexcitation. As for BR, the long-lived M-like intermediate accumulates in the microsecond time scale; however, its decay back to the original state takes ~500 ms. The formation of this species is accompanied by the protonation of an internal carboxyl group (Engelhard et al., 1996). It is probable that the light-activated *trans*/13-*cis* isomerization of retinal (Imamoto et al., 1992b) allows the transfer of the Schiff base proton to a close aspartic acid (Asp[75]). Mutation of the corresponding Asp residue in SRII from *H. salinarum* (hSRII) converts the pigment into a constitutively active photoreceptor (Spudich et al., 1997). SRII bound to its physiological transducer HtrII retards the O-decay (J. Sasaki and J. L. Spudich,

personal communication). A similar behavior has also been demonstrated for the SRI/HtrI complex (Ferrando-May et al., 1993b; Spudich and Spudich, 1993). Whether the shortened photocycle turnover of pSRII in native membranes as compared to the solubilized receptor is due to an interaction of pSRII with pHtrII (Scharf et al., 1992a) remains to be elucidated.

A comprehensive elucidation of the excitation and photocycle mechanism of the sensory rhodopsins will allow a better insight into the early steps of the signal transduction chain. In this paper the photocycle kinetics of pSRII are analyzed in the spectral range between 360 nm and 660 nm, as is their dependency upon temperature and pH. From these data, a model is proposed that displays considerable similarities to BR, with the exception of those rate constants that are connected to the M decay and the reformation of the initial state.

MATERIALS AND METHODS

Strain and plasmid

H. salinarum strain Pho81/w (BR$^-$, HR$^-$, SRI$^-$, HtrI$^-$, SRII$^-$, HtrII$^-$; kindly provided by D. Oesterhelt) was used for transformation according to the protocol of Cline et al. (1989). The *H. salinarum–E. coli* shuttle vector contained the novobiocin resistance gene (Holmes and Dyall-Smith, 1990), the *bop* promotor region (360 bp upstream from the bacterioopsin gene *bop*), as well as an extended N-terminus within the first 45 bp of the *bop* coding sequence (Ferrando-May et al., 1993a) upstream of the *psopII* gene from *Natronobacterium pharaonis* (Seidel et al., 1995). Transformants were grown on solid medium (1.5% agar-agar) in the presence of 0.4 μg/ml novobiocin (Sigma). One transformant (BL-1) contained two copies of the transformed plasmid inserted in the genomic *bop* locus (data not shown), as determined by Southern blot analysis.

Purification of pSRII

BL-1 was grown in peptone medium (4.3 M NaCl, 81 mM MgSO$_4$, 26 mM KCl, 10 mM sodium citrate, 10 g peptone/liter, pH 7.0–7.2). The cells were harvested from 20 liters of culture (OD$_{578}$ 1.8) by centrifugation and resuspended in basal salt buffer (200 ml, 4.3 M NaCl, 81 mM MgSO$_4$, 26 mM KCl, 2 mM HEPES, pH 6.5). Lysis was performed by dialysis against distilled water supplemented with 20 μg/ml DNase I for 4 h at room temperature. Membranes were collected from lysed cells by centrifugation at 100,000 $\times$ *g* for 1 h at 8°C. The pellet was subsequently washed twice with low-salt buffer (20 mM NaCl, 10 mM Tris-HCl, pH 8.0). The yield of pSRII per liter of cell culture was calculated from the washed membrane fraction, using the optical density at 500 nm (ϵ = 40,000 M^{-1} cm^{-1}), which amounted to 2.7 mg/liter cell culture. Membranes were solubilized in the dark overnight at room temperature and in the presence of 1.3% (w/v) *n*-octyl-β-D-glucopyranoside (OG).

pSRII was further purified by anion exchange chromatography on DEAE-Sepharose (CL-6B, Pharmacia) equilibrated with 50 mM NaCl, 10 mM Tris/HCl (pH 8.0), 0.65% OG. The protein was eluted with a linear gradient from 100 mM to 225 mM NaCl. Peak fractions containing pSRII were collected and used directly for reconstitution into native purple membrane lipids.

Reconstitution of pSRII into purple membrane lipids

For reconstitution of solubilized pSRII with purple membrane lipids (Krebs et al., 1995), 150 mg PM lipids were dissolved in 10 ml chloroform, and a thin lipid film on the wall of a 50-ml flask was prepared by careful evaporation of the solvent. Seven milligrams of pSRII in 25 ml 10 mM Tris-HCl (pH 7.0), 225 mM NaCl, and 0.65% (w/v) OG was added, and the suspension was gently stirred for 30 min at 30°C. The OG was removed by dialysis against a 10 mM phosphate buffer (pH 7.0) containing 230 mM NaCl. The reconstituted pSRII was pelleted twice by centrifugation at 300,000 $\times$ *g* for 1 h and resuspended in 150 mM NaCl, 10 mM Tris-HCl (pH 8.0).

Photocycle measurements

The laser flash photolysis setup was similar to that described by Chizhov et al. (1996). Transient absorption changes were recorded in a quasilog time scale from 10 ns (maximum digitizing rate) after the laser pulse (Nd:YAG, 532 nm, 10 ns, 5 mJ/cm^2) until full completion of the photocycle (20 s at 10°C). Two digital oscilloscopes (LeCroy 9361 and 9400A) were used to record the traces in two overlapping time windows. The data were acquired in steps of 5° at 12 different temperatures ranging from 10°C to 65°C. The wavelengths were varied from 360 nm to 660 nm in steps of 10 nm (all together, 31 spectral points; at 25°C the step size was 5 nm). At each wavelength, 25 laser pulses were averaged to improve the signal-to-noise ratio. Each data point was properly weighted on the basis of the baseline analysis and the quasilogarithmic data compression, as described by Chizhov et al. (1996). Absorption spectra of the samples were measured before and after each experiment.

Data evaluation

The data were analyzed according to the method of Chizhov et al. (1996). In the first step the minimal number and values of apparent rate constants were determined (four to nine exponential components were tested), using the global multiexponential nonlinear least-squares fit of the data (Müller et al., 1991; Müller and Plesser, 1991). The standard deviation of weighted residuals, their 3D surface, the temperature dependencies of the derived rate constants, and their amplitude spectra were used to determine the number of exponentials. In the second step, it was assumed that the photocycle consists of a sequence of irreversible first-order transitions. Therefore, an exact analytical solution can be applied to transform the amplitude spectra of exponents into the spectra of intermediates. Finally, the absolute absorption spectra of states were derived by varying the cycling fraction. Criteria for the determination of the cycling fraction were the absence of negative absorbency and contributions of the initial state to the derived spectra.

RESULTS

Sensory rhodopsin II from *N. pharaonis* was expressed in the *H. salinarum* strain Pho81/w. Approximately 20 mg purified pSRII could be obtained from 20 liters of cell culture. According to the ratio of the optical densities at 500 nm and 280 nm of 1:1.2, the protein sample used was quite pure and close to the value of 1:1.25 that has been extracted from the spectrum of pSRII published in Tomioka and Sasabe, 1995. Seven milligrams of pSRII was used for reconstitution into polar PM lipids (yield 65%). The absorption spectra (Fig. 1, *A* and *B*) displays the typical fine structure observed for SRII-like proteins, with the principal maximum at ~500 nm and two distinct vibronic bands at 460 nm and 420 nm. The third vibronic band at 370 nm is not directly evident from the spectra, but has been derived from the multi-Gaussian deconvolution. The second shoulder has been described for hSRII (Takahashi et al., 1990)
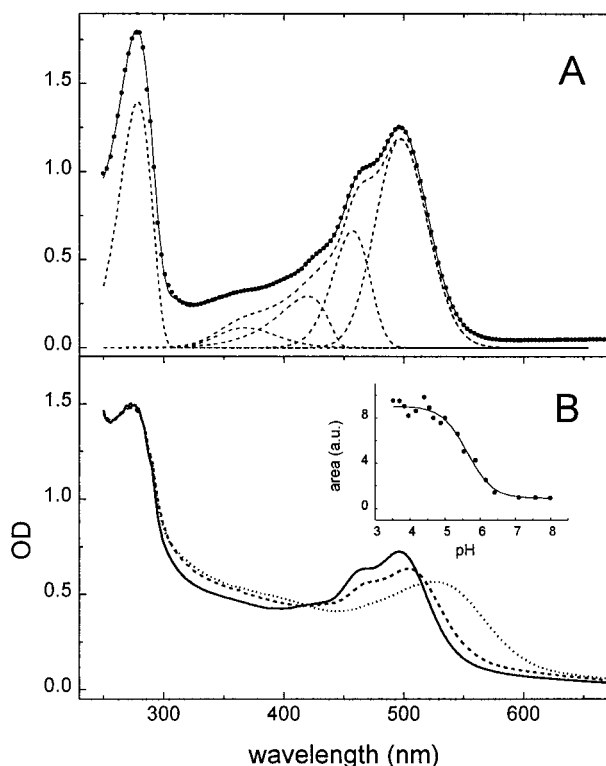
FIGURE 1 Spectrum of purified pSRII in the detergent (*A*) and membrane preparation (*B*). The result of a multi-Gaussian fit is depicted in *A* (*solid line*; *dashed lines* show the corresponding spectra of components). (*B*) Absorption spectra of pSRII at pH 8.0 (*solid line*), pH 3.0 (*dotted line*), and pH 0.5, 3 M NaCl (*dashed line*). (*Inset*) The titration curve of Asp[75] derived from the analysis of pSRII spectra recorded in the range from pH 8.0 to 3.5. Differential spectra were calculated by subtraction of the absorptions recorded at pH 8.0 from each spectrum at lower pH. The integrals of the positive differential bands were plotted against the pH, and the data were fitted by a sigmoidal function (*solid line*).

Multi-Gaussian fit of the absorption spectra of pSRII

The skewed Gaussian function with five components (four vibronic bands of the chromophore and an additional band for the aromatic absorption of the protein) has been used to fit spectral bands. This analytical formula is most suitable for describing the broad asymmetrical (because of the Franck-Condon effect) absorption spectra of retinal proteins (Scharnagl and Fischer, 1996; Birge, 1990; Metzler and Harris, 1978). The contribution of the light scattering was fitted by a power function of reciprocal wavelengths. Molar extinction coefficients (ϵ) of the chromophore states have been calculated from the coefficient of the ground spectra

and the law of conservation of particles. The skewed Gaussian function (Birge, 1990; Metzler and Harris, 1978),

$$\epsilon(\lambda) = \epsilon_{\max}$$

$$\times \exp\left\{-\frac{\ln 2}{(\ln \rho)^2}\left[\ln\left(\frac{(1/\lambda - 1/\lambda_{\max})(\rho^2 - 1)}{\Delta \nu \rho} + 1\right)\right]^2\right\},$$

$$\nu > \nu_{\max} - \frac{\Delta \nu \rho}{(\rho^2 - 1)}; \quad \epsilon(\nu) = 0, \quad \nu \leq \nu_{\max} - \frac{\Delta \nu \rho}{(\rho^2 - 1)}$$

has been used to fit spectral bands, where λ (nm) is the wavelength, $\Delta \nu$ (cm^{-1}) is the half-bandwidth, ρ is the parameter of skewness, and ϵ (M^{-1} cm^{-1}) is the molar extinction coefficient. The background scattering line has been fitted as $A + B/\lambda^C$ ($A = -0.03 \pm 0.01$, $B = (3.7 \pm 1.3) \times 10^9$, $C = 3.9 \pm 0.6$. To determine the molar extinction coefficient ϵ_{497}, the value of $\epsilon_{360} = 33,600$ M^{-1} cm^{-1} of retinaloxime (Scharf, 1992) has been used. Coefficients of all other fitted spectral bands have been calculated accordingly. All analyzed spectra (taken from detergent-solubilized and membrane-reconstituted pSRII) could be approximated by using a function with the power (*C*) close to 4, indicating that classical Rayleigh scattering of small dielectric particles occurs. In Fig. 1 *A* the ground spectrum of the pSRII in detergent is shown together with the five-component skewed Gaussian fit. The parameters of the four vibronic bands of the chromophore spectra are given in Table 2 (χ^2 is the standard deviation). The spectra of the pSRII reconstituted into lipids from the purple membrane can be fitted by similar parameters (Fig. 1 *B*), although the contribution of the light scattering is considerably higher. The maximum absorption is found at 497 nm, and the maxima of the vibronic bands are located at 457 nm, 420 nm, and 370 nm (see also Table 2), which are close to the values taken directly from the spectrum.

Titration of Asp[75]

The spectral shape and the position of the chromophore absorption band of pSRII exhibit a significant pH dependence (see Fig. 1 *B*). The absorption maximum shifts from the 500 nm, measured at physiological pH 8.0, to 525 nm (pSRII[pink]) at pH 3.5. Concomitantly, the well-pronounced vibrational fine structure is lost. A similar bathochromic shift and the loss of the fine structure are also described for the pSRII mutant D75N ($\lambda_{\max} = 522$ nm) as well as the hSRII-mutant D73N (Zhu et al., 1997). These observations may be explained by a neutralization of the Schiff base counterion, which can be accomplished either by the protonation of Asp[75] or by its mutation to Asn. It should be noted that the removal of a negative charge from the vicinity of the protonated Schiff base also leads to a bathochromic shift of the absorption maximum in the case of the other bacterial rhodopsins (Spudich et al., 1997). For example, *pharaonis* halorhodopsin, which normally absorbs at 570 nm, can be converted into a blue pigment ($\lambda_{\max} = 600$ nm)

and is evident in the spectrum of pSRII published by Imamoto et al. (1992b), as well as that of Tomioka and Sasabe (1995). The four vibronic bands are separated from each other by 1760 cm^{-1} (497 nm $\rightarrow$ 457 nm), 1990 cm^{-1} (457 nm $\rightarrow$ 420 nm), and 3440 cm^{-1} (420 nm $\rightarrow$ 367 nm), respectively.
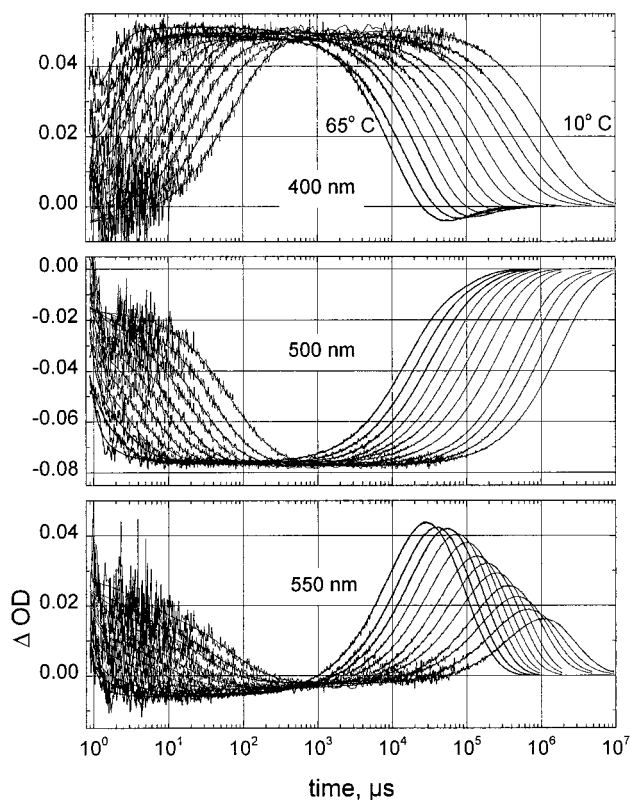
FIGURE 2 Traces of the transient absorption changes after photoexcitation of pSRII at different temperatures (from 10°C to 65°C in steps of 5°C) The time courses are shown only for selected wavelengths (400 nm, 500 nm, and 550 nm). Thin solid lines represent the result of the global fit using eight exponentials.

by abstracting the counteranion (Scharf and Engelhard, 1994). The removal of the anion from the protonated Schiff base exerts a bathochromic shift of the same order of ~900 cm^{-1} for BR, pHR, and pSRII (BR-BR^{blue}: 880 cm^{-1}, Kimura et al., 1984; pHR-bHR ^{blue}: 670 cm^{-1}, Scharf and Engelhard, 1994; pSRII-pSRII^{pink}: 940 cm^{-1}, this work and Spudich et al., 1997).

The original spectrum of pSRII with a maximum at 500 nm and a shoulder at 460 nm can almost be restored by adding 3 M NaCl to the sample and decreasing the pH to 0.5. In the presence of sulfate, this effect is not observed. A similar behavior has been described for BR (Dér et al., 1989; Fischer and Oesterhelt, 1979), and it has been proposed that the protonation of the counterion complex creates a halide binding site (Dér et al., 1991). Apparently, the counterion complex in pSRII matches that of BR, although there are subtle differences in the pK_a of the proton acceptor (BR D85; pSRII D75; see below) and its interaction with the Schiff base proton (P. Hildebrandt, personal communication).

The pK_a of Asp^{75} was determined by acid titration of reconstituted pSRII (*inset* of Fig. 1 *B*). The spectra of pSRII were recorded at 18 different pH values in the range from pH 8.0 to 3.5. Difference spectra were obtained by subtraction of the spectrum taken at pH 8.0 from those measured at lower pH values. In the inset of Fig. 1 *B*, the integrals of the

positive difference bands are plotted against the pH. The sigmoidal fit gives a pK_a of 5.6 ± 0.1. It is interesting to note that the titration curve of pSRII solubilized in dodecyl maltoside is shifted to lower pH values ($pK_a < 3$, 5, data not shown) concomitantly with a flattened slope spanning at least 4 pH units. This observation might indicate that solubilized pSRII consists of a mixture of conformationally different species. However, one could also reason that the interaction of pSRII with detergents exposes other carboxyl groups, thereby contributing to the protonation mechanism of the counterion complex.

The pK_a of Asp^{75} in reconstituted pSRII lies at 5.6, between that of the corresponding Asp residues in BR (Asp^{85}, $pK_a = 2.2$; Chang et al., 1988) and SRI (Asp^{76}, $pK_a = 7.2$; Olson et al., 1992; $pK_a = 7.4$, Haupts et al., 1995). The pK_a of Asp$^{76}_{SRI}$ increases to 8.7 upon binding of the transducer HtrI (Olson et al., 1992). The difference between the two extreme pK_a values amounts to about five units. This is accomplished by changes within the protein, although the amino acid arrangement of the extracellular channels of BR, SRI, and pSRII/hSRII seems to be quite similar (Haupts et al., 1995; Seidel et al., 1995; Grigorieff et al., 1996). How the archaeal rhodopsins tune the pK_a of their Asp residue to fulfill the functional requirements is certainly an interesting question and needs further study.

Multiexponential global analysis

In Fig. 2 the experimentally measured transient absorbency changes of the pSRII photocycle and their multiexponential fit (see below) are depicted at three characteristic wavelengths (400 nm, 500 nm, and 550 nm). Traces are shown for different temperatures ranging from 10°C to 65°C in steps of 5°C. The light-triggered absorbance changes were analyzed from ~1 μs to 10 s, which encompasses seven orders of magnitude. The traces at 500 nm depict the depletion and recovery of the original ground state, whereas the records at 400 nm are indicative of the deprotonation and reprotonation of the Schiff base. The 550 nm traces display a temperature-dependent increase of absorbency toward the end of the photocycle, pointing to the formation of a red-shifted intermediate. After the initial reactions, the protein rests for almost three orders of magnitude of time before decaying back to the initial state.

The whole data set was analyzed by the global nonlinear multiexponential fitting program (MEXFIT) (Chizhov et al., 1996; Müller and Plesser, 1991). Each temperature point was treated independently. This analysis provided eight kinetic components, which can describe the photocycle at temperatures below 35°C. From 35°C to 65°C the fastest time constant could not be resolved. Criteria for determining the number of kinetic components were 1) the mean value of weighted residuals (standard deviation) that saturated as the number was increased from eight to nine (Chizhov et al., 1996) (see Fig. 3; the small decrease in standard deviation at the nine exponential approximation is
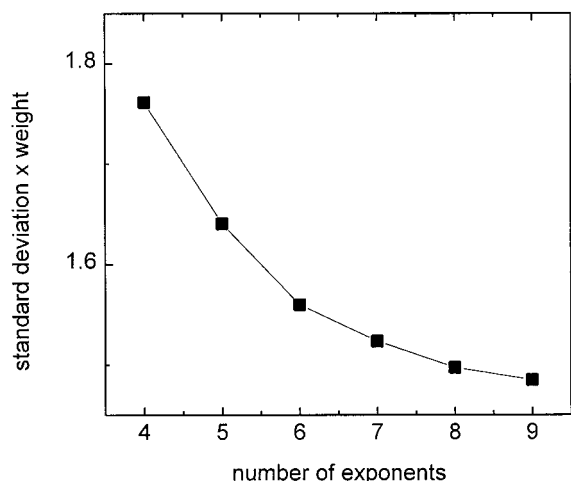
FIGURE 3 Dependence of the standard deviation of the weighted residuals upon the number of exponents used for the global fit of data. Each point of the curve represents the mean value from the fits of the photocycle kinetics at the 11 temperature points.

due to the fit of the temperature-independent laser artifact, which has a half-time of ~100 ns); 2) a smooth Arrhenius behavior of the derived rate constants (Fig. 4); and 3) the temperature evolution of the corresponding amplitude spectra (Fig. 5). Furthermore, eight exponentials were also found

to be sufficient for the analysis of the pH dependence and the D_2O dependence of the pSRII photocycle (Fig. 4), showing that the relaxational pathway does not change under these conditions.

The rate constants resolved in the present study partially agree with those of published work (Scharf et al., 1992b; Imamoto et al., 1992b; Miyazaki et al., 1992) in which components giving rise to major amplitude changes have been detected. For these rate constants, half-life times of ~1 μs, ~30 μs, ~500 ms, and ~1.5 s have been determined at 20°C, which correspond to τ_1 (1 μs) and τ_8 (1.5 s), as well as to a combination of τ_2 with τ_3 (30 μs) and τ_5 with τ_6 and τ_7 (500 ms).

Temperature dependence of rate constants

The Arrhenius plots of the apparent rate constants are shown in Fig. 4 A. The corresponding apparent activation parameters are given in Table 1. The first three components (τ_1 to τ_3) are connected to the formation of the long-lived M-like intermediate, which is characterized by a deprotonated Schiff base. τ_1 could only be resolved at the four lower temperatures. These three relaxational components have almost the same values of half-times and slopes in the Arrhenius plot as the corresponding exponentials of the BR
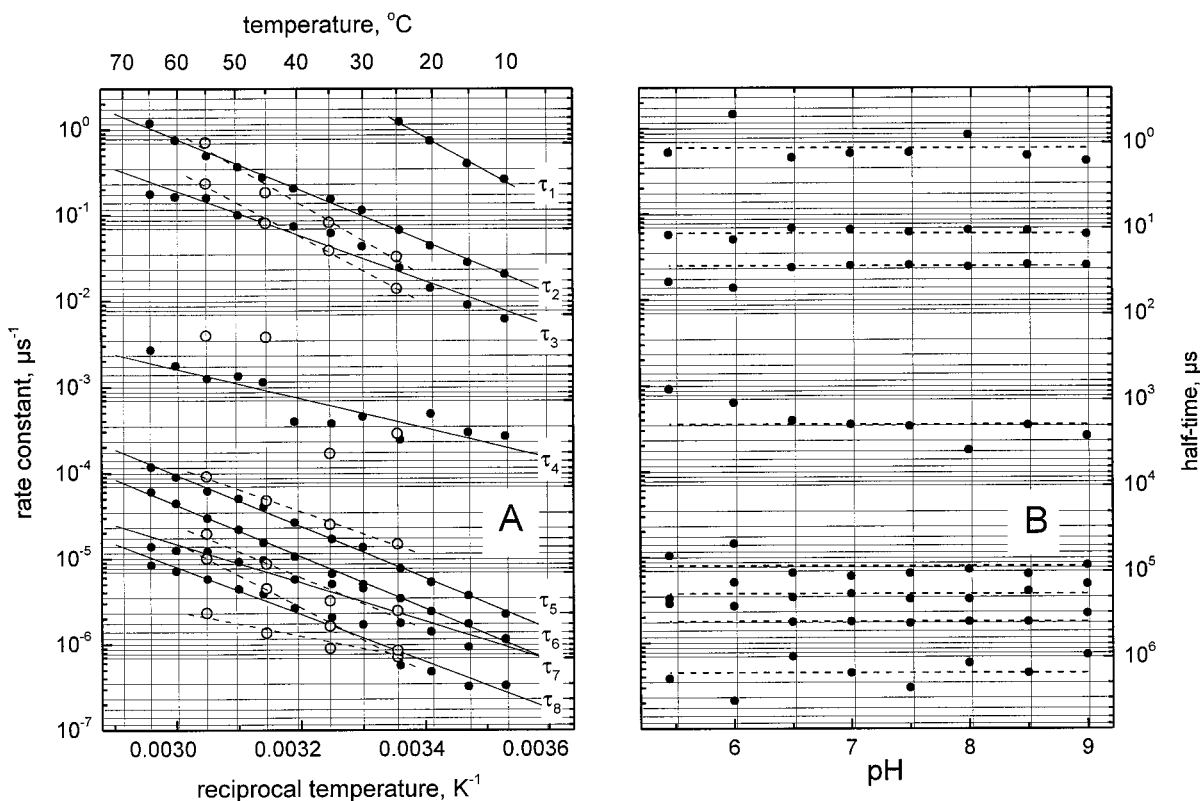

FIGURE 4 Temperature dependence (A) and pH dependence (B) of the apparent rate constants derived from an eight-exponential global fit. The rate constants shown in the Arrhenius plot (A) were determined in H_2O at pH 8.0 (●) and in D_2O at pD 8.0 (○). Straight lines in A represent the least-squares fit of the apparent activation parameters (see Table 2) according to the Eyring equation. Dashed lines in B are drawn to guide the eye. The horizontal grid lines correspond to the right (half-times) axis, and the vertical grid lines in A to the top (°C) axis.
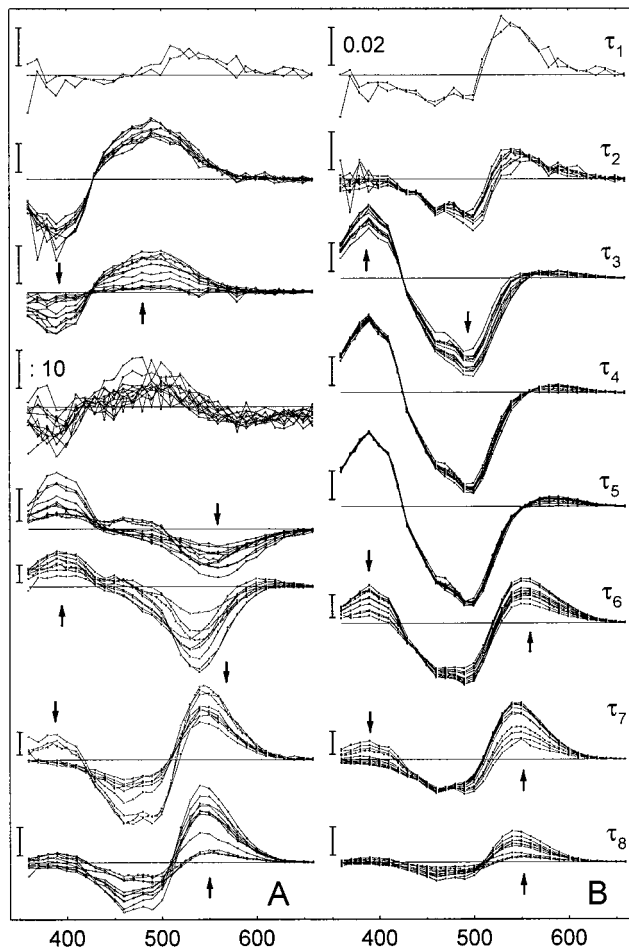
FIGURE 5 Temperature dependencies of the differential spectra of amplitudes of eight exponents (τ_1 to τ_8) (*A*) and corresponding differential spectra of the kinetically distinct states (*B*). The latter spectra were derived from the spectra of exponents, assuming an irreversible sequential scheme of transitions. The figure shows the experimental data (*points*) and the Gaussian fit (*solid lines*) of the absorption spectrum of the initial state and those of the kinetic states P_1–P_8, which were fitted globally at all measured temperatures. See Table 2 for the parameters of the fitted spectra. The arrows indicate the direction for increasing temperatures.

photocycle. The reprotonation of the Schiff base and the reformation of the original ground state occur in four steps of closely spaced time constants (τ_5 to τ_8). These components of relaxation are ~100 times slower than those connected to the M decay of the BR photocycle (Chizhov et al., 1996). It should be noted that the Arrhenius behavior of τ_3 and τ_7 deviates systematically from linear dependence, as approximated in Fig. 4 *A*. The slight positive curvature of these two rate constants is indicative of an influence of a preceding temperature-dependent quasiequilibrium. However, a preceding quasiequilibrium does not necessarily lead to a nonlinear Arrhenius dependence (see, e.g., τ_6 in Fig. 4 *A*). This issue has been analyzed in more detail by Chizhov et al. (1996).

To fit the data properly, an additional component (τ_4) has to be introduced between the two major parts of the pSRII photocycle, the formation and decay of $pSRII_{400}$, which are

separated by three orders of magnitude. Although the amplitudes of this transition are rather small compared to those of the other components (Fig. 5 *A*), this relaxation has been found to be significant at all measured temperatures, at different pH values, as well as upon D_2O substitution. The small amplitudes could be explained by an intermediate that does not belong to the main relaxational path, or by a relaxation between two states that are almost identical spectrally. Because of the small amplitudes, the thermodynamic parameters could only be approximated (Table 1).

It is important to note that the multiexponential fit of relaxational kinetics does not permit fully statistically independent nonlinear parameters (rate constants) to be obtained. Therefore, errors in the thermodynamic parameters given in Table 1 are underestimated. From a comparison of the photocycle data of BR (Chizhov et al., 1996) with the present results, it can be concluded that the distribution of the observed half-times of the relaxation from ~1 μs to ~10 ms (BR) or 1 s (pSRII) is obtained mainly by a decrease in the entropic part of the activation barriers (from ~40 J/mol K to −40 J/mol K in BR or to −80 J/mol K in pSRII), whereas the enthalpic components match each other (~50 kJ/mol).

The effect of D_2O on the pSRII photocycle was measured at four representative temperatures (25°C, 35°C, 45°C, and 55°C). Under these conditions, the first component τ_1 could not be resolved; however, all of the other seven rate constants were identified. The deuteration of the sample has little effect on the first part of the photocycle (τ_1 to τ_3), which is connected to the deprotonation of the Schiff base. On the other hand, the rates of the second half of the photocycle (τ_6 to τ_8) decrease by a factor of ~2. This result differs from the D_2O effect in BR, which has recently been published (Dickopf and Heyn, 1997; Le Coutre and Gerwert, 1996). In these papers it was described that the H_2O/D_2O exchange slows down the first part of the photocycle by a factor of 5, whereas the reformation of the initial state is decelerated as in pSRII, by a factor of only 2.

pH dependence of rate constants

In Fig. 4 *B* the eight rate constants of the pSRII photocycle are plotted against the pH of the buffer. As is obvious from this figure, the photocycle kinetics are almost unaffected in the pH range between pH 5.5 and pH 9.0. Because of a pK_a of the pSRII → $pSRII^{pink}$ transition of 5.6, contributions from the latter species are already discernible at pH 5.5 (data not shown), which will become dominant at pH < 5.5. Contrary to the above results, Miyazaki et al. (1992) reported a pH dependency (below pH 7) of one of the two slow components (k_1). The apparent pK_a determined from the pH dependency of k_1 is close to that found for Asp[75] (see Fig. 1 *B*). Therefore, the apparent discrepancies might be explained by the contribution of the acid form of pSRII to the kinetics. However, it might also be possible that the

TABLE 1 Apparent activation parameters of the pSRII photocycle

	τ_1	τ_2	τ_3	τ_4	τ_5	τ_6	τ_7	τ_8
H_2O								
$\Delta H^{\#}$ (kJ/mol)	74 ± 4	55 ± 1	48 ± 3	30 ± 4	55 ± 1	55 ± 1	41 ± 3	50 ± 3
$\Delta S^{\#}$ (J/mol K)	120 ± 15	31 ± 1	30 ± 4	-94 ± 10	-43 ± 3	-49 ± 3	-102 ± 11	-78 ± 10
D_2O								
$\Delta H^{\#}$ (kJ/mol)		76 ± 9	70 ± 5	85 ± 38	46 ± 3	55 ± 10	69 ± 2	24 ± 7
$\Delta S^{\#}$ (J/mol K)		98 ± 28	72 ± 17	85 ± 121	-68 ± 9	-55 ± 30	-17 ± 7	-166 ± 21

different conditions used for measuring the kinetics (pSRII reconstituted into PM lipids and low ionic strength (this study) versus solubilized pSRII at high ionic strength; Miyazaki et al., 1992) are responsible for the apparent discrepancies.

Differential spectra of exponents and intermediates

The differential amplitude spectra corresponding to the eight exponents and their temperature dependencies are depicted in Fig. 5 *A*. In this representation, positive amplitudes denote the decay and negative amplitudes an increase in transient absorptions with respect to the initial and/or the final state of pSRII. As mentioned above, eight exponents are necessary to generate smooth spectra and to describe their dependencies on temperature. As already discussed, the amplitude changes connected to τ_4 are rather small compared to the other transitions.

Assuming a sequential irreversible chain of transitions $P_1 \rightarrow P_2 \rightarrow \ldots P_8 \rightarrow P_0$, the differential spectra of kinetic states P_i (intermediates) can be obtained from the spectra of exponents (Fig. 5 *B*) by direct algebraic deconvolution (Chizhov et al., 1996). The intrinsic rate constants of this model were assigned to the experimentally observed rate constants in descending order. Possible permutations of intrinsic and experimental rate constants were tested, but they led to unreasonable absolute spectra of states. It is interesting to note that the amplitude spectra and the corresponding differential spectra of intermediates generally do not resemble each other. Therefore, it is not possible to extrapolate reliably from amplitude spectra directly to the absolute spectra of intermediates.

Absolute spectra of kinetic states (P_i)

The absolute absorbance spectra of the kinetic states (P_1 to P_8) were obtained by adding the differential spectra to the ground spectrum of pSRII and by optimizing the cycling fraction, which is the single unknown of the model. The cycling fraction was varied from 1 to 0 until no contribution of the initial state and/or negative absorbance could be observed. Within the whole range of altered parameters (i.e., temperature, pH, H_2O/D_2O) and at fixed parameters of the laser excitation of pSRII (see Materials and Methods), the cycling fraction was found to be $11 \pm 1\%$. This low number is due to the excitation wavelength of the laser. At 532 nm the extinction is only ~30% of the maximum value at 500 nm.

The absolute spectra of the kinetic states P_i are depicted in Fig. 6. Each panel combines the spectra of kinetic states for each temperature point with the ground spectrum of the pSRII. The absolute spectra have been approximated by a multi-Gaussian fit whose parameters are summarized in Table 2 (see also the fitted curves (*solid lines*) in Fig. 6). Four kinetic states (P_1, P_2, P_4, and P_5) have almost temperature-independent spectra with a single maximum at 510 nm, 495 nm, 400 nm, respectively. These kinetic states can be interpreted as pure (irreducible) spectral intermediates, and by comparing their appearance and relative spectral position with the intermediates of the BR photocycle, one can describe them as K-, L-, and M-like spectral intermediates ($pSRII_{510}$, $pSRII_{495}$, $pSRII_{400}$, respectively). It is obvious from the absorption maxima that two M-like intermediates exist (P_4 and P_5), which are connected by the spectrally silent transition τ_4. The spectra of the other states P_3, P_6, P_7, and P_8 are temperature dependent. Moreover, they represent fast equilibria between different spectral intermediates. In P_3 a temperature-dependent equilibrium is established between spectral states absorbing at 495 nm ($pSRII_{495}$) and 400 nm ($pSRII_{400}$). At the lowest temperature measured (10°C), the ratio of $pSRII_{495}$ to $pSRII_{400}$ approaches 0.25:0.75. At 65°C this equlibrium is shifted completely to $pSRII_{400}$. P_6 and P_7 constitute components of the photocycle that are characterized by various concentrations of M-, N-, and O-like species in equilibrium with one another. It should be noted that the normalized sums of the species at all kinetic states are always close to unity, thus indicating that the assumption of quasiequilibria is valid.

The kinetic state P_8 has the longest lifetime (1.2 s at 25°C) of all intermediates. It represents an equilibrium of $pSRII_{535}$ (and probably $pSRII_{485}$) with a state possessing a spectrum identical to that of the initial state. For BR, a similar slowly decaying intermediate has been described. It was argued that this component belongs to the 13-*cis* retinal photocycle (Chizhov et al., 1996). However, this explanation does not seem to be true for τ_8, because the apoprotein of pSRII does not bind 13-retinal; hence a light/dark adaptation does not occur (Hirayma et al., 1995).
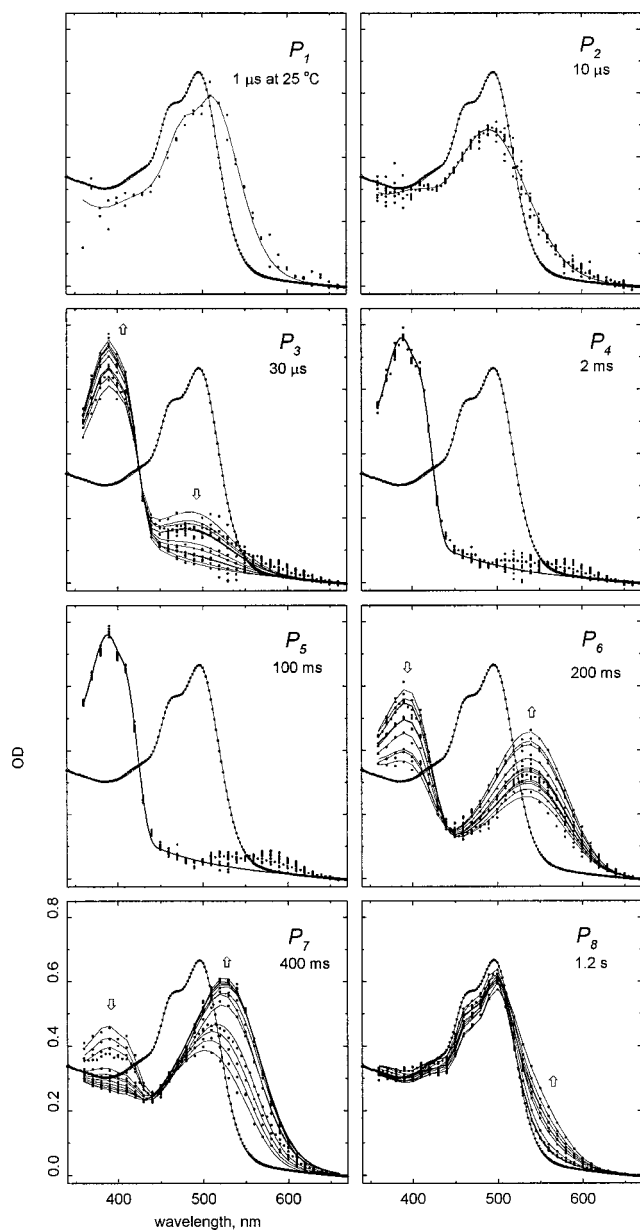
FIGURE 6 Absolute spectra of kinetic states P_1–P_8 at temperatures between 10°C and 65°C (step size 5°C, pH 8). The arrows indicate the direction of increasing temperatures. Depicted half-times of transitions correspond to 25°C. For reasons of comparison, the spectrum of pSRII is also shown in each panel. The figure shows the experimental data (*points*) and the Gaussian fit (*solid lines*) of the absorption spectra of the initial state and those of the kinetic states P_1–P_8, which were fitted globally at all measured temperatures. The spectra of the first state (P_1; K-like intermediate) could only be resolved at 10°C and 15°C. The spectra were derived from the difference spectra of the kinetic states (see Fig. 5 *B*) by variation of the cycling fraction. Over the whole temperature range, the value of the cycling fraction is 11 ± 1% (note that the wavelength of the laser excitation (532 nm) is far from the absorption maximum of pSRII (500 nm)).

Absolute spectra of archetypal chromophore states (S_j)

The absolute spectra of the eight kinetic states P_i (Fig. 6) were fitted simultaneously for all temperatures points by a

TABLE 2 Parameters of the Gaussian fit of the spectra of the pSRII photocycle in Figs. 6 and 7

	$\epsilon_{max} \times 10^{-4}$ $(M^{-1}\ cm^{-1})$	ρ	$\Delta\nu$ (cm^{-1})	λ_{max} (nm)
S_{01}	3.85 ± 0.06	1.00 ± 0.06	2015 ± 152	497.0 ± 1.3
S_{02}	2.3 ± 0.3	1.26 ± 0.25	1735 ± 333	457.5 ± 3.1
S_{03}	1.1 ± 0.4	1.8 ± 0.4	2808 ± 1722	419 ± 15
S_{04}	0.3 ± 0.4	1.0 ± 1.5	3790 ± 3000	371 ± 26
χ^2 0.0001				
S_{11}	3.5 ± 0.1	1.0 ± 0.3	2620 ± 850	511 ± 6
S_{12}	1.6 ± 0.2	1.6 ± 2.4	2256 ± 6090	466 ± 50
S_{13}	0.6 ± 3	1.3 ± 1.9	3500 ± 6000	417 ± 110
χ^2 0.009				
S_{21}	2.7 ± 0.02	1.13 ± 0.07	4000 ± 270	493 ± 1.5
S_{22}	0.8 ± 0.1	1.2 ± 0.2	4010 ± 400	404 ± 4.5
χ^2 0.002				
S_{31}	3.4 ± 0.1	1.65 ± 0.25	3265 ± 930	403 ± 4
S_{32}	0.95 ± 0.8	1.9 ± 0.4	3237 ± 880	377 ± 4
χ^2 0.001				
S_4	4.1 ± 0.4	1.58 ± 0.04	3917 ± 102	486 ± 2
S_5	4.4 ± 0.2	1.13 ± 0.02	2719 ± 55	536 ± 1.5
χ^2 0.0002				

multi-Gaussian function. The spectra of the chromophore states (S_j, $j = 1$–5) could be extracted from the results; these are shown in Fig. 7 (together with the spectrum of the initial state S_0). The corresponding spectral parameters are presented in Table 2. As can be seen, the eight kinetic states P_i consist of only five irreducible chromophore states S_j, which are temperature independent in the measured range from 10°C to 65°C. In the photocycle of pSRII, the first emerging chromophore state S_1 absorbs at 510 nm and has a shoulder at ~470 nm. These properties—early appearance and bathochromic shift of the absorption maximum—are congruent to those of the K intermediate of the BR photocycle. The next state S_2 shows similarities to the L-intermediate. Furthermore, the other chromophore states S_3, S_4, and S_5 show parallels to M_{410}, N_{550}, and O_{640} of the BR photocycle, with respect to the sequence of their appearance and the relative spectral shifts of their absorption maxima. It should be noted that the fine structure of the pSRII chromophore states is preserved in S_1, S_2, and S_3; however, it seems that in S_4 and S_5 this feature is lost. However, this might also be due to the spectral and kinetic overlapping of S_4 and S_5.

Despite differences in the rates and absorption maxima, the general features of the pSRII and BR chromophore states are strikingly similar. Apparently, the isomerization of the retinal chromophore triggers conformational changes in both proteins, as well as alterations of charge patterns, which allow only for a limited number of archetypal spectra. This is somewhat surprising, because the pigments have different functional roles. BR, as efficient proton pump, has had to optimize the proton transfer chains and switch the separating cytoplasmic and extracellular access to the Schiff base. On the other hand, pSRII is primed to alter its surface in the signaling state, which has to be recognized by the transducer to relay the signal to CheA. A common property
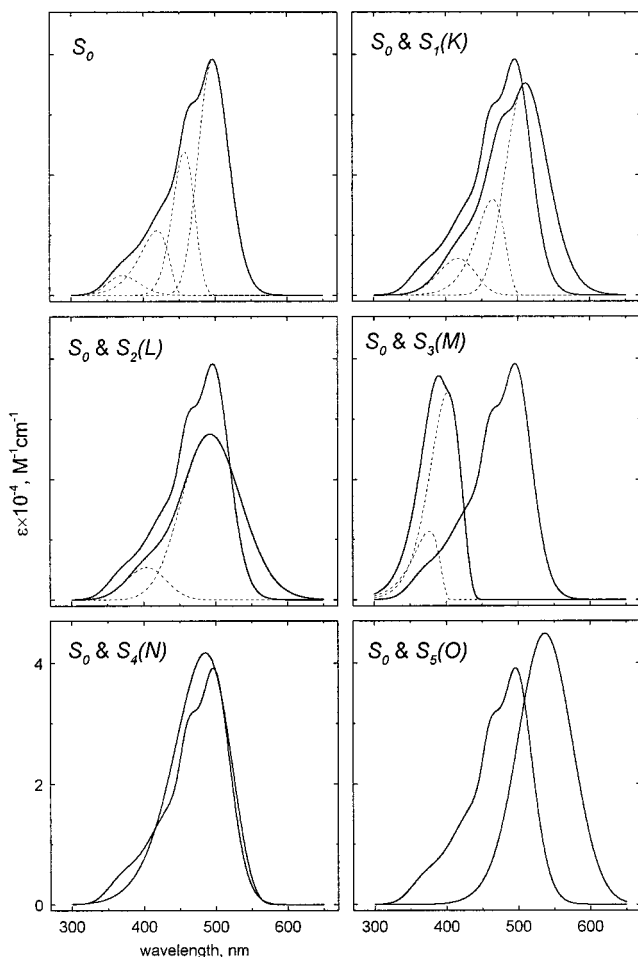
FIGURE 7   Spectra of the pSRII chromophore in the initial state S_0, and those deduced from the global spectral fitting of the data in Fig. 6 (S_1–S_5). The dotted lines represent the vibronic subbands. The spectral data are compiled in Table 2, in which the double indices denote the corresponding subbands.

FIGURE 8   Model of the pSRII photocycle.

of the two pigments is their ability to pump protons (E. Bamberg, personal communication). Therefore, pSRII must also undergo a switch, changing the cytoplasmic or extracellular accessibility of the Schiff base. It is tempting to speculate that this event also triggers the physiological response.

CONCLUSIONS

The analysis of the photocycle of the bacterial rhodopsins and their mutants under various conditions has been and certainly remains an important tool for the investigation of the physiological function of the pigments (for reviews on the photocycle of BR and HR, see Oesterhelt, 1995; Lanyi and Váró, 1995). One aim of the present study and that of a previous paper (Chizhov et al., 1996) was to establish procedures to obtain standardized data bases. These should meet the requirement of being applicable not only to visible absorption changes as in the present work, but also to other biophysical methods that produce time-dependent signal
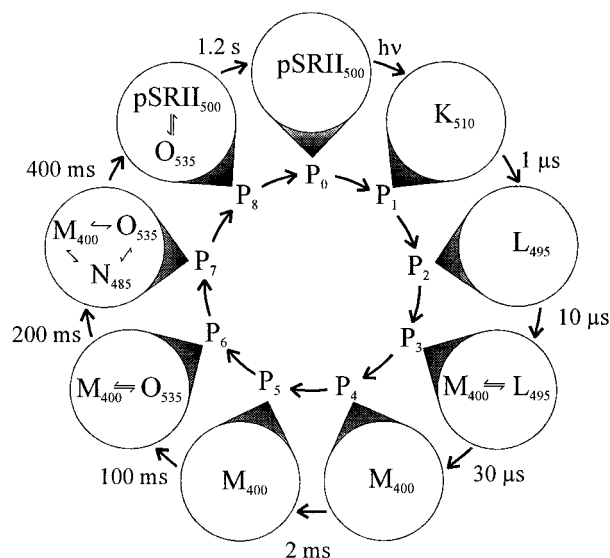
changes, like, e.g., time-resolved FTIR (Lohrmann et al., 1994) or current measurements (Müller et al., 1991). In the first step, the number of exponentials of a given process has to be determined. These are only accurately available if the data set fulfills certain qualifications: 1) The signal-to-noise ratio should be of sufficient quality. 2) The number of observables should be greater than one. The more independent measurements that are performed, the better the interpretation. 3) A very important point concerns the measurements at different temperatures, because it makes it possible to distinguish between physically meaningful kinetic and spectral components, and it will also improve resolution. Of course, it also reveals the thermodynamics of the process. 4) Alteration of external parameters such as pH, ionic strength, and/or H_2O/D_2O exchange can greatly enhance the quality of the data set and will provide further evidence of the number of exponentials describing the process.

Our present analysis and the comparison with the photocycles of BR and pHR indicate that the distribution of relaxation times from ~1 μs to tens of milliseconds (BR, pHR) or even seconds (pSRII) is mainly due to the change of entropic part of the apparent activation barriers, which varies from about +40 J/mol K to −40 J/mol K (BR, pHR) or −80 J/mol K (pSRII), whereas the enthalpic part of barriers (~50 kJ/mol) stays approximately constant. It is interesting to note that the latter value corresponds to the "universal" currency of many protein enzymatic activities that are "fueled" by the ATP hydrolysis. In our case the process is initiated by the photon excitation, but rate-limiting steps of the relaxation are probably driven by similar protein dynamic modes.

In the case of BR and pSRII, the number of exponentials (τ_i, $i = 1 \ldots n$) has to be reconciled with the number of spectroscopically determined intermediates (S_j, $j = 1 \ldots m$). In both examples, m equals 5 and is less than n (BR: $n = 7$; pSRII: $n = 8$). At this point the assumption of a unidirec-

tional irreversible scheme was made, which led to kinetic states P_i that resembled not only archetypal chromophore states (S_j), but also the equilibria between them. This treatment of the data provided a valid description not only of the photocycles of BR and pSRII, but also of that of HR (I. Chizhov et al., manuscript in preparation). Furthermore, it also allows the influence of external variables and/or mutations on the photocycle parameters to be analyzed (e.g., time constants and/or shifts of equilibria).

It is of particular importance that the interaction of the transducer pHtrII with pSRII can now be studied in greater detail. Spudich and Spudich (1993) have demonstrated that the binding of the transducer (SRI) of sensory rhodopsin I increases the turnover rate of the photocycle. Sasaki and Spudich have shown that the interaction of hSRII with its transducer hHtrII decreases the rate of the O decay (J. Sasaki and J. L. Spudich, personal communication). In a recent paper Yan et al. (1991) analyzed the signaling state of SRII. The authors concluded that the M-like intermediate and/or the late intermediates represent a conformation that is responsible for the signal transduction. It is expected that a thorough elucidation of the effects of transducer binding on the photocycle of pSRII will provide evidence for the physiologically active states.

REFERENCES

Birge, R. R. 1990. Nature of the primary photochemical events in rhodopsin and bacteriorhodopsin. *Biochim. Biophys. Acta Bio-Energetics.* 1016:293–327.

Chang, C. H., R. Jonas, R. Govindjee, and T. G. Ebrey. 1988. Regeneration of blue and purple membranes from deionized bleached membrane of *Halobacterium halobium. Photochem. Photobiol.* 47:261–265.

Chizhov, I., D. S. Chernavskii, M. Engelhard, K. H. Müller, B. V. Zubov, and B. Hess. 1996. Spectrally silent transitions in the bacteriorhodopsin photocycle. *Biophys. J.* 71:2329–2345.

Cline, S. W., L. C. Schalkwyk, and W. F. Doolittle. 1989. Transformation of the archaebacterium *Halobacterium volcanii* with genomic DNA. *J. Bacteriol.* 171:4987–4991.

Dér, A., S. Száraz, R. Tóth-Boconádi, Z. Tokaji, L. Keszthelyi, and W. Stoeckenius. 1991. Alternative translocation of protons and halide ions by bacteriorhodopsin. *Proc. Natl. Acad. Sci. USA.* 88:4751–4755.

Dér, A., R. Tóth-Boconádi, and L. Keszthelyi. 1989. Bacteriorhodopsin as a possible chloride pump. *FEBS Lett.* 259:24–26.

Dickopf, S., and M. P. Heyn. 1997. Evidence for the first phase of the reprotonation switch of bacteriorhodopsin from time-resolved photovoltage and flash photolysis experiments on the photoreversal of the m-intermediate. *Biophys. J.* 73:3171–3181.

Eisenbach, M. 1996. Control of bacterial chemotaxis. *Mol. Microbiol.* 20:903–910.

Engelhard, M., B. Scharf, and F. Siebert. 1996. Protonation changes during the photocycle of sensory rhodopsin II from *Natronobacterium pharaonis. FEBS Lett.* 395:195–198.

Ferrando-May, E., B. Brustmann, and D. Oesterhelt. 1993a. A C-terminal truncation results in high-level expression of the functional photoreceptor sensory rhodopsin I in the archaeon *Halobacterium salinarum. Mol. Microbiol.* 9:943–953.

Ferrando-May, E., M. Krah, W. Marwan, and D. Oesterhelt. 1993b. The methyl-accepting transducer protein HtrI is functionally associated with the photoreceptor sensory rhodopsin I in the archaeon *Halobacterium salinarum. EMBO J.* 12:2999–3005.

Fischer, U., and D. Oesterhelt. 1979. Chromophore equilibria in bacteriorhodopsin. *Biophys. J.* 28:211–230.

Grigorieff, N., T. A. Ceska, K. H. Downing, J. M. Baldwin, and R. Henderson. 1996. Electron-crystallographic refinement of the structure of bacteriorhodopsin. *J. Mol. Biol.* 259:393–421.

Haupts, U., C. Haupts, and D. Oesterhelt. 1995. The photoreceptor sensory rhodopsin I as a two-photon-driven proton pump. *Proc. Natl. Acad. Sci. USA.* 92:3834–3838.

Hirayama, J., Y. Imamoto, Y. Shichida, N. Kamo, H. Tomioka, and T. Yoshizawa. 1992. Photocycle of phoborhodopsin from haloalkaliphilic bacterium (*Natronobacterium pharaonis*) studied by low-temperature spectrophotometry. *Biochemistry.* 31:2093–2098.

Hirayama, J., N. Kamo, Y. Imamoto, Y. Shichida, and T. Yoshizawa. 1995. Reason for the lack of light-dark adaptation in *pharaonis* phoborhodopsin: reconstitution with 13-*cis*-retinal. *FEBS Lett.* 364:168–170.

Hoff, W. D., K. H. Jung, and J. L. Spudich. 1997. Molecular mechanism of photosignaling by archaeal sensory rhodopsins. *Annu. Rev. Biophys. Biomol. Struct.* 26:223–258.

Holmes, M. L., and M. L. Dyall-Smith. 1990. A plasmid vector with a selectable marker for halophilic archaebacteria. *J. Bacteriol.* 172:756–761.

Imamoto, Y., Y. Shichida, J. Hirayama, H. Tomioka, N. Kamo, and T. Yoshizawa. 1992a. Chromophore configuration of *pharaonis* phoborhodopsin and its isomerization on photon absorption. *Biochemistry.* 31:2523–2528.

Imamoto, Y., Y. Shichida, J. Hirayama, H. Tomioka, N. Kamo, and T. Yoshizawa. 1992b. Nanosecond laser photolysis of phoborhodopsin: from *Natronobacterium pharaonis* appearance of KL and L intermediates in the photocycle at room temperature. *Photochem. Photobiol.* 56:1129–1134.

Imamoto, Y., Y. Shichida, T. Yoshizawa, H. Tomioka, T. Takahashi, K. Fujikawa, N. Kamo, and Y. Kobatake. 1991. Photoreaction cycle of phoborhodopsin studied by low-temperature spectrophotometry. *Biochemistry.* 30:7416–7424.

Kimura, Y., A. Ikegami, and W. Stoeckenius. 1984. Salt and pH-dependent changes of the purple membrane absorption spectrum. *Photochem. Photobiol.* 40:641–646.

Krebs, M. P., E. N. Spudich, and J. L. Spudich. 1995. Rapid high-yield purification and liposome reconstitution of polyhistidine-tagged sensory rhodopsin I. *Protein Expr. Purif.* 6:780–788.

Lanyi, J. K., and G. Váró. 1995. The photocycles of bacteriorhodopsin. *Isr. J. Chem.* 35:365–385.

Le Coutre, J., and K. Gerwert. 1996. Kinetic isotope effects reveal an ice-like and a liquid-phase-type intramolecular proton transfer in bacteriorhodopsin. *FEBS Lett.* 398:333–336.

Lohrmann, R., T. Althaus, W. Eisfeld, and M. Stockburger. 1994. Light-induced reaction sequence of the chromophore in bacteriorhodopsin. Studied by time-resolved RR spectroscopy. *In* Time-Resolved Vibrational Spectroscopy VI. A. Lau, F. Siebert, and W. Werncke, editors. Springer-Verlag, Berlin and Heidelberg. 208–214.

Metzler, D. E., and C. M. Harris. 1978. Shapes of spectral bands of visual pigments. *Vision Res.* 18:1417–1420.

Miyazaki, M., J. Hirayama, M. Hayakawa, and N. Kamo. 1992. Flash photolysis study on pharaonis phoborhodopsin from a haloalkaliphilic bacterium (*Natronobacterium pharaonis*). *Biochim. Biophys. Acta Bio-Energetics.* 1140:22–29.

Müller, K.-H., H. J. Butt, E. Bamberg, K. Fendler, B. Hess, F. Siebert, and M. Engelhard. 1991. The reaction cycle of bacteriorhodopsin: an analysis using visible absorption, photocurrent and infrared techniques. *Eur. Biophys. J.* 19:241–251.

Müller, K.-H., and T. Plesser. 1991. Variance reduction by simultaneous multi-exponential analysis of data sets from different experiments. *Eur. Biophys. J.* 19:231–240.

Oesterhelt, D. 1995. Structure and function of halorhodopsin. *Isr. J. Chem.* 35:475–494.

Olson, K. D., P. Deval, and J. L. Spudich. 1992. Absorption and photochemistry of sensory rhodopsin. I. pH effects. *Photochem. Photobiol.* 56:1181–1187.

Scharf, B. 1992. Vergleichende Untersuchungen des sensorischen Rhodopsins II in *Halobacterium halobium* und *Natronobacterium pharaonis* und Charakterisierung des Halocyanins des ersten blauen Kupferproteins aus Archaebakterien. Thesis/Dissertation. Ruhr-Universtät, Bochum, Germany.

Scharf, B., and M. Engelhard. 1994. Blue halorhodopsin from *Natronobacterium pharaonis*: wavelength regulation by anions. *Biochemistry.* 33:6387–6393.

Scharf, B., B. Hess, and M. Engelhard. 1992a. Chromophore of sensory rhodopsin II from *Halobacterium halobium. Biochemistry.* 31:12486–12492.

Scharf, B., B. Pevec, B. Hess, and M. Engelhard. 1992b. Biochemical and photochemical properties of the photophobic receptors from *Halobacterium halobium* and *Natronobacterium pharaonis. Eur. J. Biochem.* 206:359–366.

Scharnagl, C., and S. F. Fischer. 1996. Conformational flexibility of arginine-82 as source for the heterogeneous and pH-dependent kinetics of the primary proton transfer step in the bacteriorhodopsin photocycle—an electrostatic model. *Chem. Phys.* 212:231–246.

Seidel, R., B. Scharf, M. Gautel, K. Kleine, D. Oesterhelt, and M. Engelhard. 1995. The primary structure of sensory rhodopsin II: a member of an additional retinal protein subgroup is coexpressed with its transducer, the halobacterial transducer of rhodopsin II. *Proc. Natl. Acad. Sci. USA.* 92:3036–3040.

Shichida, Y., Y. Imamoto, T. Yoshizawa, T. Takahashi, H. Tomioka, N. Kamo, and Y. Kobatake. 1988. Low-temperature spectrophotometry of phoborhodopsin. *FEBS Lett.* 236:333–336.

Spudich, E. N., and J. L. Spudich. 1993. The photochemical reactions of sensory rhodopsin I are altered by its transducer. *J. Biol. Chem.* 268:16095–16097.

Spudich, E. N., W. S. Zhang, M. Alam, and J. L. Spudich. 1997. Constitutive signaling by the phototaxis receptor sensory rhodopsin II from disruption of its protonated Schiff base Asp-73 interhelical salt bridge. *Proc. Natl. Acad. Sci. USA.* 94:4960–4965.

Takahashi, T., B. Yan, P. Mazur, F. Derguini, K. Nakanishi, and J. L. Spudich. 1990. Color regulation in the archaebacterial phototaxis receptor phoborhodopsin (sensory rhodopsin II). *Biochemistry.* 29:8467–8474.

Tomioka, H., and H. Sasabe. 1995. Isolation of photochemically active archaebacterial photoreceptor, pharaonis phoborhodopsin from *Natronobacterium pharaonis. Biochim. Biophys. Acta Bio-Membr.* 1234:261–267.

Yan, B., T. Takahashi, R. Johnson, and J. L. Spudich. 1991. Identification of signaling states of a sensory receptor by modulation of lifetimes of stimulus-induced conformations: the case of sensory rhodopsin II. *Biochemistry.* 30:10686–10692.

Yao, V. J., and J. L. Spudich. 1992. Primary structure of an archaebacterial transducer, a methyl-accepting protein associated with sensory rhodopsin I. *Proc. Natl. Acad. Sci. USA.* 89:11915–11919.

Zhang, W. S., A. Brooun, M. M. Mueller, and M. Alam. 1996. The primary structures of the archaeon *Halobacterium salinarum* blue light receptor sensory rhodopsin II and its transducer, a methyl-accepting protein. *Proc. Natl. Acad. Sci. USA.* 93:8230–8235.

Zhu, J. Y., E. N. Spudich, M. Alam, and J. L. Spudich. 1997. Effects of substitutions D73E, D73N, D103N and V106M on signaling and pH titration of sensory rhodopsin II. *Photochem. Photobiol.* 66:788–791.